Optimizing surfactant templating of yttria-stabilized zirconia aerogels for high-temperature applications: Effect of cationic surfactant

Rebecca C. Walker[a], Jamesa L. Stokes[b], Frances I. Hurwitz[b†], Haiquan Guo[c], James K. Ferri[a]*

[a]*Department of Chemical & Life Science Engineering, Virginia Commonwealth University, Richmond, VA, USA*

[b]*NASA Glenn Research Center, Cleveland, OH, USA*

[c]*Universities Space Research Association, Cleveland, OH, USA*

*Corresponding author: jkferri@vcu.edu, 601 West Main Street, Room 403, Box 843028, Richmond, Virginia 23284-3028

[†]Retired

Abstract

Aerogels can be used in spaceflight applications as thermal insulators due to their low density, low thermal conductivity, and tortuous path for solid conduction. However, the aerogel formulation must be optimized to increase the thermal stability of the aerogels, as a drastic densification and decrease in surface area often is exhibited after high-temperature exposure. This work considers yttria-stabilized zirconia (YSZ) aerogels, which have low thermal conductivity and are expected to be used for temperatures between 600°C and 1000°C. It is anticipated that new sol-gel chemistries will yield YSZ aerogels that exhibit retained mesoporous structure, increased surface area, and minimized shrinkage upon exposure to higher temperatures in the expected use range. This work investigates the addition of surfactant to 20 mol% YSZ aerogels. The cationic surfactant, cetrimonium bromide (CTAB), was used as the templating agent, preventing the collapse of the mesoporous structure upon gelation and drying. It was determined that adding one-half times the critical micelle concentration of CTAB increased the surface area of the

aerogels by 72% and 41% and increased the pore volume following exposure to 600°C and 1000°C, respectively. This level of CTAB had the greatest increase in surface area and pore volume as compared to aerogels without CTAB or with twice the critical micelle concentration of CTAB. By optimizing the concentration of CTAB, the thermal stability of YSZ aerogels can be enhanced to make these materials more efficient when used as thermal management systems.

Keywords

Yttria-stabilized zirconia aerogel; material optimization; mesoporous structure; cationic surfactant templating; thermal management

1. Introduction

Aerogels are a unique class of mesoporous solid materials that exhibit a wide range of useful properties, including high surface area, low density, and low thermal conductivity. Aerogels are the lightest synthetic material in the world, composed of 95 - 99% air by volume. The extreme material properties of aerogels make them useful for many applications, including thermoresisters, sensors, catalysis, sorption media, drug delivery, and electrodes in solid oxide fuel cells [1–7]. Due to having low thermal conductivities and an overall mesoporous and lightweight structure, the use of aerogels in thermal management systems is also promising, with applications including insulation, fire suits or blankets, aerospace, and aeronautics [8–13]. Silica aerogels, which are well-known and well-studied, suffer from sintering and densification when exposed to temperatures

above 700°C due to polycondensation reactions and structural rearrangement [14,15]. The pore structure and high surface area of the aerogel upon high-temperature exposure is required to leverage the benefits of aerogel properties in thermal management systems. Therefore, the collapse of the pore structure and decrease of surface area diminishes the utility of the material as a thermal insulator.

One of the ways that the densification and surface area reduction of aerogels can be mitigated during high-temperature exposure is by using surfactants to template the aerogels during sol-gel synthesis. Surfactants can be used as structure directing agents to control the pore structure of materials in the mesopore range, from 2 to 50 nm, such as aerogels [2]. Surfactants, composed of a hydrophilic head and a hydrophobic tail, can influence the properties of synthesized aerogels such as pore size, surface area, and crystallinity through electrostatic repulsion and steric hindrance effects [16]. Furthermore, surfactants are known to reduce interfacial energy, a major cause of surface tension in the aerogel system, which can lead to pore collapse and cracking during the drying process [17]. Surfactants can also be used as capping agents in the aerogel system, controlling nanoparticle size and reducing aggregation, which can lead to aerogels with greater surface area values.

Certain types of surfactants are known to form spherical micelles at or above the critical micelle concentration (CMC) of the surfactant [18]. By adding surfactants to the aerogel solution prior to gelation, the precursor particles will aggregate around the micelles and, following the addition of the gelation agent, the gel will begin to form. When the gels are exposed to temperatures above 350°C, either through drying to form aerogels or post-processing heat-treatment, the surfactants are oxidized and burned off, leaving behind

tunable, uniform pores within the aerogel. The surfactant templating process is depicted in **Scheme 1**. It is hoped that by templating aerogel pores with surfactants, pore structure and high surface area will be maintained when aerogels are exposed to high temperatures. It should be noted that while surfactants aid in templating aerogel pores, not all the pores are templated from the surfactant micelles and instead result from the aggregation of the solid precursor particles and the subsequent formation of the gel network.

In this paper, we explore the use of a surfactant templating agent to control the porosity of yttria-stabilized zirconia (YSZ) aerogels. Zirconia aerogels were first known to be synthesized by a non-alkoxide, epoxide addition sol-gel route by Chervin et al. in 2005 [19]. Typically, zirconia aerogels have lower surface areas than silica aerogels, 200 – 900 m^2/g for zirconia aerogels versus 500 – 1200 m^2/g for silica aerogels, and higher thermal conductivities than silica aerogels, 0.021 – 0.180 W/m·K for zirconia aerogels versus 0.012 – 0.020 W/m·K for silica aerogels [20,21]. These properties alone would make silica aerogels more favorable for use in thermal management systems than zirconia aerogels. However, because of the high melting point of zirconium dioxide, 2715°C, zirconia aerogels can remain stable at high temperatures between 600°C and 1000°C, whereas silica aerogels begin to sinter and densify at temperatures between 500°C and 700°C, collapsing the pore structure [14,22]. Adding yttrium to the zirconia system also makes these materials advantageous as, even when not in aerogel form, the YSZ system is thermally stable; the addition of yttrium stabilizes the tetragonal zirconia phase, which prevents transformation to the monoclinic phase, thereby lowering the thermal conductivity of the system (2.2 – 2.9 W/m·K) [13,23]. By making YSZ into aerogels, this thermal conductivity

is further decreased to be as low as 0.168 W/m·K by leveraging the high porosity and high surface area properties of the aerogels. We expect that by adding surfactant to the formulation of the aerogels during sol-gel synthesis, we can control the pore structure of the aerogels and we can attenuate the negative effects, such as densification and decrease of surface area, due to heat-treatment.

We optimize the YSZ aerogel formulation, including the type and amount of surfactant added, to reduce the negative effects associated with high-temperature exposure. The cationic surfactant, cetrimonium bromide (CTAB), was chosen as the surfactant template in this study. In the sol-gel synthesis of alumina-zirconia nanopowders, Rezaee et al. determined that the addition of CTAB synthesized smaller nanoparticles with narrow size distribution and higher surface areas as compared to nanoparticles synthesized with nonionic surfactants [16]. As an example specifically relating to zirconia aerogels, Jung et al. found that in the synthesis of ambient pressure dried zirconia aerogels, the addition of CTAB increased the specific surface area of the aerogels by up to 89% [17]. High surface area was retained after annealing at 400°C, indicative of an enhanced thermal stability of the aerogels synthesized with CTAB. When dissolved in solvent, CTAB is known to release cations that can interact with the zirconia matrix. The cationic charges lead to an induced repulsive force between collections of zirconia during the drying process, which can prevent shrinkage of the pore system caused by capillary forces. The repulsive forces between the cation and the zirconia matrix are ultimately the cause of increased surface area in zirconia aerogels templated with CTAB. The addition of CTAB also improves the emulsification of the sol, leading to a more homogenous resulting material. Additionally,

CTAB discourages agglomeration and controls particle geometry by adsorbing onto the surface of precursor particles. However, the adsorption of CTAB on the aerogel matrix by electrostatic attraction is also known to decrease the skeleton strength of the aerogel, which can lead to shrinkage during drying. Interestingly, Sai et al. determined that small amounts of CTAB increased pore size and volume of silica aerogels, while larger amounts of CTAB reduced pore size and volume [24]. Huang et al. demonstrated a similar result where larger concentrations of CTAB led to smaller pores and weakened skeletons in silica aerogels [25]. Therefore, the amount of CTAB must be optimized to mitigate pore shrinkage, surface area loss, densification, and sintering, which will enhance the mesoporous structure of the aerogel. The combination of the YSZ system with the addition of surfactant to control the pore structure of the aerogels makes these materials promising for use in thermal management systems, specifically for aeronautics and aerospace applications. The optimization of aerogels used in these applications will lead to increased effectiveness and thermal stability of the systems up to temperatures of 1000°C.

2. Experimental

Yttria-stabilized zirconia (YSZ) aerogels were synthesized, as depicted in **Scheme 1**, using a similar sol-gel procedure to the one used by Hurwitz et al. [26]. Zirconyl chloride octahydrate, $ZrOCl_2 \cdot 8H_2O$, (Alfa Aesar, 99.9% metals basis) and yttrium(III) chloride hexahydrate, $YCl_3 \cdot 6H_2O$, (Acros Organics, 99.9%) were used as the zirconium and yttrium precursors, respectively. The precursors were mixed with the solvents, ethanol (Decon Labs, 200 proof) and deionized water, to create the sol. To minimize experimental variables in this paper, a value of 20 mol% for yttria content was chosen because this mole

ratio retained mesoporous structure and smaller particle size after high-temperature exposure compared with lower dopant levels in prior work completed by Hurwitz et al. [26]. Higher yttria content was also shown to increase the thermal stability of YSZ aerogels [27]. Regarding water content, twice the stoichiometric amount was chosen, as this water level was shown to synthesize aerogels with higher surface area and pore volume at high temperature than other water levels following experimentation.

Prior to gelation, the chosen surfactant, cetrimonium bromide, CTAB, (MP Biomedicals) was added to the sol as a multiple of the surfactant's critical micelle concentration (CMC). The CMC of CTAB varies when ethanol is added to the solution; the CMC increases as the ethanol volume fraction increases. This change in CMC was taken into account in the YSZ aerogel formulations, as CMC values of CTAB at varying ethanol fractions were estimated from a thermodynamic model [28]. The addition of the inorganic salts $ZrOCl_2 \cdot 8H_2O$ and $YCl_3 \cdot 6H_2O$ was determined to have a negligible effect on the CMC of CTAB, as the decrease in CMC due to the salt addition was shielded by the large increase of the CMC due to the ethanol addition. For these experiments, the effect of ethanol on the CMC values of CTAB was considered only. To determine the influence of different concentrations of CTAB on the aerogel pore structure, 0.5x the CMC of CTAB and 2x the CMC of CTAB were added to the formulations. The molar ratio of CTAB to inorganic precursors was 0.13 for 0.5x CTAB and 0.50 for 2x CTAB.

To initiate gelation, the gelation agent, propylene oxide (Sigma Aldrich, ReagentPlus, 99%), was used. Immediately after the addition of propylene oxide, the sol was poured into the aerogel molds; gelation typically occurred within 10 minutes. After 24

hours of aging, the gel was washed in 200 proof ethanol for 5 – 7 days to allow ethanol to fill the pores of the gel. The gel was then supercritically dried using carbon dioxide. The supercritical drying process exchanged the solvent in the gel's pores with air, transforming the gel into an aerogel. Following drying, a selection of the aerogels were heat-treated in high-purity alumina boats under flowing argon at temperatures of 600°C, 1000°C, and 1100°C for 18 minutes. The ramp rate of the tube furnace was 5°C/min.

As-dried and heat-treated aerogels were then characterized using a variety of techniques. As-dried shrinkage and density were determined through physical measurement using a digital caliper. Scanning electron microscopy was performed using a Hitachi SU-70 FE-SEM and a Hitachi S-4700 FE-SEM to show, qualitatively, the effects of surfactant on microstructure. The SEM samples were uncoated and imaged at 1 – 2 kV with a working distance of 4.5 – 5.0 mm. Nitrogen adsorption/desorption was conducted on a Micromeritics ASAP 2020 Plus instrument and a Micromeritics ASAP 2020 instrument; surface area of the aerogels was determined using the BET method of Brunauer–Emmett–Teller and the pore size distribution was determined from the desorption isotherm using the BJH method of Barrett-Joyner-Halenda. The analysis accounts for open pores less than 100 nm in size only. Following the measurement, pore size distributions of the aerogel samples were determined by plotting the pore volume (cm^3/g) as a function of the pore diameter (nm). An Empyrean Multipurpose X-Ray Diffractometer was used to determine surfactant effects on crystalline phase transformation and average crystallite size for heat-treated aerogels. Cu Kα radiation was used with a wavelength of 1.54059 Å from 10° to 90° 2θ. Profile fitting in HighScore and the cubic

phase YSZ powder diffraction file (PDF) reference card were used to analyze the aerogel samples. To determine the average crystallite size for each sample, the Scherrer equation, the Monshi-Scherrer (M-S) method, the Williamson-Hall (W-H) method, and the Size-Strain-Plot (SSP) method were used [29]. Transmission electron microscopy was conducted using a JEOL JEM-F200 Cold FEG Electron Microscope with an accelerating voltage of 200 kV to confirm the effects of surfactant on crystallite size.

3. Results and Discussion

In this paper, we aim to use surfactant templating to retain the pore structure and high surface area of yttria-stabilized zirconia (YSZ) aerogels upon high-temperature exposure so that the benefits of aerogel properties can be leveraged for use in thermal management systems. We expect that CTAB will increase the surface area, pore volume, and pore size of as-dried YSZ aerogels. In addition, it is anticipated that the addition of CTAB will attenuate the decrease of the surface area and pore volume accompanying heat-treatment of the aerogels. The mesoporous structure of YSZ aerogels suppresses gas convection due to the small pore size, but the retention of open pore volume is critical for reducing solid conduction through the material. Successful surfactant templating of YSZ aerogels should improve the effectiveness of these materials when used in the expected use range of 600°C to 1000°C.

Physical measurements taken after supercritical drying were used to determine the as-dried shrinkage and density of the YSZ aerogels. The as-dried shrinkage is the percent change of the as-dried aerogel monolith diameter with respect to the original diameter of the gelation mold. It was determined that the as-dried shrinkage increased as the CTAB

level was increased. The shrinkage was 17 ± 1% for aerogels without CTAB, 20 ± 1% for 0.5x CTAB aerogels, and 25 ± 1% for 2x CTAB aerogels. While added CTAB increased the as-dried shrinkage, 2x CTAB was shown to have the greater increase. This effect could have been the result of a reduction in the skeleton strength of the aerogel at higher CTAB amounts, which is further elaborated below. The density remained approximately constant when the amount of CTAB was changed: 0.26 ± 0.01 g/cm^3 at 0x CTAB, 0.25 ± 0.01 g/cm^3 at 0.5x CTAB, and 0.25 ± 0.01 g/cm^3 at 2x CTAB.

Fig. 1 displays the pore size distributions of the YSZ aerogels at different levels of CTAB. **Fig. 1A** is at 0x CTAB, **Fig. 1B** is at 0.5x CTAB, and **Fig. 1C** is at 2x CTAB. Three different heat-treatment conditions are displayed on each plot and represented as different marker shapes: as-dried (circle), 600°C for 18 min (square), and 1000°C for 18 min (diamond). Considering the aerogel samples that were not heat-treated, the aerogel without CTAB had a pore size distribution between 0 nm and 40 nm, while the aerogels with 0.5x CTAB and 2x CTAB had wider pore size distributions within 0 nm and 80 nm and within 0 nm and 55 nm, respectively. **Fig. 1** showed that aerogels heat-treated at 600°C had similar pore sizes, regardless of CTAB content. At 600°C, the pore size distributions ranged from 5 to 35 nm with major distributions at 18 nm. For aerogels heat-treated at 1000°C, the pore size distributions ranged from 10 to 35 nm with the major pore size distributions shifting to smaller pore sizes with increasing CTAB amount, from 28 nm (0x CTAB) to 22 nm (0.5x CTAB) and 18 nm (2x CTAB). As a templating agent, the micelle size of CTAB can be affected by many factors, such as concentration, temperature, and pH [30]. CTAB forms micelles with diameters of 2 to 3 nm in water. In this study, the

precursor solution, prior to the addition of CTAB, had a pH of 1. At this pH, it is estimated according to the work reported by Patel et al. describing the influence of solution pH on the size of CTAB micelles that the hydrodynamic diameter of CTAB is approximately 25 nm, which is closer to the measured pore size distribution of the aerogels [31]. It should be noted that, since nitrogen adsorption/desorption only measures pores less than 100 nm, the actual distribution could have included pores that were greater than 100 nm but were not measured by nitrogen adsorption/desorption. No macroporosity was observed in the SEM images of the as-dried samples, which are not displayed here. Because of this, it was determined that the distribution seen in nitrogen adsorption/desorption was representative of the range of pore sizes in the sample.

The BET surface area (m^2/g) and BJH desorption cumulative pore volume (cm^3/g) values are displayed in **Table 1**. The addition of CTAB was shown to increase the surface area of the as-dried YSZ aerogels, with 0.5x CTAB and 2x CTAB increasing the surface area by 53% and 55%, respectively. Once the aerogels were heat-treated, the surface areas were shown to decrease, which was indicative of sintering following high-temperature exposure. However, the addition of CTAB was shown to increase the surface area of the aerogels at 600°C and 1000°C. At 600°C, the addition of 0.5x CTAB and 2x CTAB increased the surface area by 72% and 21%, respectively, while at 1000°C, the surface area increased by 41% with 0.5x CTAB and by 27% with 2x CTAB. The addition of CTAB was shown to increase pore volume compared to the aerogels without CTAB, with 0.5x CTAB displaying higher pore volumes than 2x CTAB. Aerogels with 0.5x CTAB and 2x CTAB displayed a decrease in pore volume as heat-treatment temperature increased, which

was expected due to sintering and densification. However, the aerogels with 0.5x CTAB had larger pore volumes at 600°C and 1000°C than the aerogels without CTAB and with 2x CTAB. Specifically, the addition of 0.5x CTAB was shown to enable the retention of a measurably larger total pore volume following heat-treatment at 600°C and 1000°C than the aerogels without CTAB or with 2x CTAB.

The addition of 0.5x CTAB was shown to be more effective at inhibiting surface area decrease and pore collapse following high-temperature exposure as aerogels with 0.5x CTAB showed the overall highest surface area and pore volume following heat-treatment. The larger pore volume would most likely lower the solid conduction of the aerogel, enhancing the use of the aerogel as a thermal insulator. This result was surprising, as it was expected that a larger amount of CTAB would more effectively template the aerogel pores. This result could have been influenced by the estimation of the critical micelle concentration of CTAB. The effect of ethanol was considered when estimating the CMC values; however, other factors, including the inorganic salt concentration, could have influenced the CMC, but were not considered in the estimate. The pore size distribution in **Fig. 1** was narrower at 0.5x CTAB than at 2x CTAB for as-dried aerogels, pointing to a more homogenous pore structure during synthesis, and suggesting that 0.5x CTAB may have been closer to the actual CMC.

Alternatively, the addition of 2x CTAB could have had a negative effect on the surface area and pore volume of the heat-treated aerogels because a larger amount of surfactant was detrimental to the aerogel structure. This is supported by the study conducted by Sai et al. which determined that, at higher amounts, the polar head groups of

CTAB may have interacted with the zirconia domains, adsorbing onto the aerogel backbone by electrostatic attraction [17,24]. The steric hindrance caused by this adsorption could have constrained the gelation reaction, causing a reduction of the skeleton strength of the gel and leading to increased shrinkage during drying.

Scanning electron microscopy (SEM) was used to determine the pore structure of the YSZ aerogels and how it was affected by high-temperature exposure. **Fig. 2** displays SEM images of YSZ aerogels with 0x CTAB (**Fig. 2A, B**), 0.5x CTAB (**Fig. 2C, D**), and 2x CTAB (**Fig. 2E, F**) levels following heat-treatment at 600°C for 18 min (**Fig. 2A, C, E**) and at 1000°C for 18 min (**Fig. 2B, D, F**). Sintering and densification of the pore structure of the as-dried aerogels without CTAB were evident following high-temperature exposure, especially noticeable at 1000°C. This behavior was expected and is typical for metal oxide materials exposed to high temperatures. With the addition of CTAB, the aerogel structures are less dense or coarse than those without, especially at 1000°C. It was expected that the addition of CTAB would template distinct pores within the aerogel structure, even after exposure to 1000°C. However, differences of the pore size in aerogels without CTAB and aerogels with CTAB were difficult to distinguish. While a slight shift in pore size can be observed, it is difficult to assign statistical significance to the difference.

X-ray diffraction (XRD) was used to determine the crystalline phase transformation and crystallite size following heat-treatment of YSZ aerogels with different amounts of CTAB. **Fig. 3** displays the XRD patterns of YSZ aerogels at different surfactant levels and heat-treatment conditions. The aerogel that was not heat-treated was non-crystalline or amorphous; this was true for all as-dried samples, regardless of CTAB loading. The

aerogel samples that were heat-treated at 600°C and 1000°C were all crystalline, regardless of CTAB content. The XRD patterns in **Fig. 3** for the YSZ aerogels without CTAB showed increased crystallinity with heat-treatment. The as-dried sample had very broad peaks, indicative of an amorphous structure, while the sample heat-treated at 600°C displayed sharper, more defined peaks, exhibiting some crystallization of the material. It was determined from these patterns that the YSZ aerogel transformed from an amorphous structure to a crystalline structure by 600°C. When comparing to the sample at 600°C, the 0x CTAB sample that was heat-treated at 1000°C displayed even sharper and more defined peaks, possibly indicative of increased crystallite size following exposure to increased temperatures. When considering **Table 1**, it was determined that increasing crystallite size was accompanied by a decrease of surface area and pore volume.

Following analysis, it was determined that the peaks for all the heat-treated samples were indicative of the cubic YSZ crystalline phase. This was expected as, based on the YSZ phase diagram, the cubic phase should be the primary phase for samples with 20 mol % Y at temperatures up to 2500°C [32]. There may have been small amounts of the tetragonal YSZ phase mixed with the cubic phase; however, the cubic peaks overlapped with the tetragonal peaks on the pattern, which made the presence of the tetragonal phase hard to determine. The addition of CTAB was shown to have no effect on the crystalline phase of the YSZ aerogels. **Table 2** displays the average crystallite size of the YSZ aerogel samples in this study. The Scherrer equation, the conventional method for determining the crystallite size of particles, can only be utilized for crystallite sizes up to 1000 Å and often has error associated with it due to the instrument signal and noise. Therefore, as a way to

compare the results of the Scherrer equation, the Monshi-Scherrer (M-S) method, the Williamson-Hall (W-H) method, and the Size-Strain-Plot (SSP) method were also utilized [29]. At 600°C, the average crystallite size was smaller for each level of CTAB than the crystallite size at 1000°C. At 1000°C, the crystallite size was the smallest in YSZ aerogels with CTAB, as compared to the aerogel without CTAB.

Due to certain limitations and error associated with the XRD equations, TEM was conducted to confirm the values estimated from the XRD analysis. **Fig. 4** displays the TEM images of YSZ aerogels with 0x CTAB (**Fig. 4A**), 0.5x CTAB (**Fig. 4B**), and 2x CTAB (**Fig. 4C**) that were heat-treated at two different conditions: 600°C and 1000°C (inset). As shown in the figure, the aerogels heat-treated at 600°C and 1000°C all appeared to display some crystallization, with the aerogels at 1000°C displaying larger crystallites than the aerogels at 600°C. Analysis of the TEM images determined that the average size of the crystallite particles, displayed in **Table 2**, increased by 343% at 0x CTAB, 197% at 0.5x CTAB, and 176% at 2x CTAB when the temperature was increased from 600°C to 1000°C, further indicating that exposure to higher temperatures increased the crystallite size. This behavior was expected as heat-treatment is known to promote crystallization of the YSZ aerogels and to increase growth of the crystallite particles. Additionally, in **Fig. 4**, the aerogel without CTAB appeared to have crystallites larger than the aerogels with CTAB at 1000°C. The TEM analysis confirmed the XRD results, which determined that the average crystallite size was smaller at 600°C than at 1000°C, as well as smaller in aerogels with CTAB than the aerogel without CTAB at 1000°C. It was determined that the addition of CTAB to the YSZ aerogels inhibited crystallite growth at 1000°C, which may

have hindered surface area and pore volume decrease, as well as shrinkage, at high temperatures. YSZ aerogels with CTAB may show increased effectiveness when used in high-temperature applications if crystallite growth, and accompanying surface area and pore volume decrease, can be impeded.

To further determine the effect of high-temperature exposure on aerogels without and with CTAB, selected aerogel samples were heat-treated at 1100°C for 18 min. **Fig. 5** displays the SEM images of YSZ aerogel samples with 0x CTAB (**Fig. 5A**) and 2x CTAB (**Fig. 5B**) that were heat-treated at 1100°C. The BET surface area and BJH desorption cumulative pore volume values are displayed below each sample. Heat-treatment at 1100°C was shown to cause further sintering and densification, in addition to larger particle growth, of the aerogels, as compared to the heat-treatment at 600°C and 1000°C displayed in **Fig. 2**. The effect of CTAB was not distinctly apparent in the SEM images of the 0x CTAB and 2x CTAB aerogels. The YSZ aerogels without CTAB had a surface area and pore volume of 11 m^2/g and 0.01 cm^3/g, respectively, following exposure to 1100°C. For aerogels exposed to the same temperature with 2x CTAB, the surface area and pore volume were 21 m^2/g and 0.02 cm^3/g, respectively. These results demonstrate that there was significant collapse of the pore structure at 1100°C. In order to extend the use range for these materials, the formulation must be further optimized so that pore collapse and subsequent densification are mitigated. This optimization may include investigating different surfactant types or concentrations, as well as yttria and water loading, to extend the use range of these materials above 1000°C. Future work may also increase the heat-

treatment time to further elucidate the effect of high-temperature exposure on the pore structure of YSZ aerogels.

Based on this study, it was determined that 0.5x CTAB was an effective amount of CTAB to use as a surfactant template in YSZ aerogels as compared to 2x CTAB. This is in agreement with the study conducted by Sai et al. with silica aerogels which determined that smaller amounts of CTAB increased the pore size and pore volume of the aerogels [24]. The surface area of aerogels with 0.5x CTAB was higher following exposure to 600°C and 1000°C than aerogels without CTAB or with 2x CTAB. In addition, the pore volume at 0.5x CTAB was larger for both as-dried and heat-treated (600°C and 1000°C) aerogels than the pore volume of aerogels without CTAB and with 2x CTAB. The addition of CTAB releases cations, which attach to the zirconia aerogel network, potentially inducing a repulsive force and effectively reducing shrinkage of the pore structure during drying [17]. The mitigation of shrinkage overall increases the surface area and pore volume of the aerogels following high-temperature exposure, allowing these materials to be used as effective thermal insulators.

However, following this investigation, it was believed that at the increased level of 2x CTAB, the higher concentration of cationic surfactant may have been negatively influencing the pore structure, which could have included a reduction in surface area and pore volume [24]. Cationic surfactants are known to adsorb onto the negatively charged surface sites of minerals through electrostatic attractions, often forming a dense electrical double layer at the solid-liquid interface [33]. When the concentration of surfactant increases, the hydrocarbon chains of the surfactants begin to aggregate and form two-

dimensional structures called hemicelles. We hypothesize that at the higher concentration of CTAB, the strength of the gelled matrix was decreased, making it more susceptible to shrinkage during drying and heat-treatment and reducing the surface area and pore volume of the aerogels. Similar interactions have been known to occur between CTAB and silica aerogels through settling of the polar head groups of CTAB towards the silica domain [34,35]. Additionally, CTAB is known to interact with negatively charged copper(II) hydroxide during the templating of cuprite nano-whiskers; this interaction influences the structure and morphology of the final nano-materials [36]. YSZ aerogels with 2x CTAB exhibited decreased surface area and pore volume following high-temperature exposure as compared to aerogels with 0.5x CTAB; this surprising behavior may have been a result of the adsorption of CTAB, which may have impeded the extent of the gelled network.

Future work investigates the specific interactions of surfactants with the zirconia matrix using ex-situ experiments with cationic, anionic, and nonionic structure formers. Enhanced understanding of the interactions of surfactants with the zirconia matrix will lead to the selection of more effective surfactant templates for aerogels. The surfactants can then be used in-situ to determine the success as a templating agent through synthesis and characterization of the aerogel system. Surfactant templates should prevent pore collapse of the mesoporous structure and promote high surface area of the aerogel upon high-temperature exposure.

4. Conclusions

The addition of the cationic surfactant, cetrimonium bromide (CTAB), was shown to influence the mesoporous structure and surface area of 20 mol% Y, 2x H_2O yttria-

stabilized zirconia (YSZ) aerogels. However, it was critical that the amount of CTAB used was optimized so that it was used at an amount that was low enough to inhibit interactions with the zirconia aerogel matrix that may have caused a reduction in surface area and pore volume yet high enough to be advantageous for surfactant templating. It was established following this study that 0.5x the critical micelle concentration (CMC) of CTAB was an ideal concentration for effective surfactant templating. The addition of 0.5x CTAB synthesized aerogels with higher surface area and pore volume following exposure to 600°C and 1000°C, as compared to aerogels without CTAB or with 2x the CMC of CTAB. It is hoped that optimized surfactant templating will lead to the synthesis of YSZ aerogels with increased thermal stability. These materials will then be more efficient when used in thermal management systems in the expected use range of 600°C to 1000°C for a variety of applications, including aeronautics and aerospace applications.

Acknowledgements

The authors would like to acknowledge Dr. Massimo Bertino (Virginia Commonwealth University) for TEM imaging. The authors would like to acknowledge NASA Fellowship 80NSSC18K1697 for financial support of this work.

References

[1] A. Feinle, N. Hüsing, Mixed metal oxide aerogels from tailor-made precursors, J. Supercrit. Fluids. 106 (2015) 2–8. https://doi.org/10.1016/j.supflu.2015.07.015.

[2] U.K.H. Bangi, H.-H. Park, Evolution of textural characteristics of surfactant-mediated mesoporous zirconia aerogel powders prepared via ambient pressure drying route, Int. Nano Lett. 8 (2018) 221–228. https://doi.org/10.1007/s40089-018-0241-7.

[3] Y. Lee, J.W. Choi, D.J. Suh, J.M. Ha, C.H. Lee, Ketonization of hexanoic acid to diesel-blendable 6-undecanone on the stable zirconia aerogel catalyst, Appl. Catal. A Gen. 506 (2015) 288–293. https://doi.org/10.1016/j.apcata.2015.09.008.
[4] H. Maleki, Recent advances in aerogels for environmental remediation applications: A review, Chem. Eng. J. 300 (2016) 98–118. https://doi.org/10.1016/j.cej.2016.04.098.
[5] Z. Ulker, C. Erkey, An emerging platform for drug delivery: Aerogel based systems, J. Control. Release. 177 (2014) 51–63. https://doi.org/10.1016/j.jconrel.2013.12.033.
[6] J. Stergar, U. Maver, Review of aerogel-based materials in biomedical applications, J. Sol-Gel Sci. Technol. 77 (2016) 738–752. https://doi.org/10.1007/s10971-016-3968-5.
[7] B. Liu, M. Gao, X. Liu, Y. Xie, X. Yi, L. Zhu, X. Wang, X. Shen, Monolithic zirconia aerogel from polyacetylacetonatozirconium precursor and ammonia hydroxide gel initiator: formation mechanism, mechanical strength and thermal properties, RSC Adv. 8 (2018) 41603–41611. https://doi.org/10.1039/C8RA08263D.
[8] I. Smirnova, P. Gurikov, Aerogel production: Current status, research directions, and future opportunities, J. Supercrit. Fluids. 134 (2018) 228–233. https://doi.org/10.1016/j.supflu.2017.12.037.
[9] A. Shaid, L. Wang, R. Padhye, M.A.R. Bhuyian, Aerogel nonwoven as reinforcement and batting material for firefighter's protective clothing: a comparative study, J. Sol-Gel Sci. Technol. 87 (2018) 95–104. https://doi.org/10.1007/s10971-018-4689-8.
[10] N. Bheekhun, A.R. Abu Talib, S. Mustapha, R. Ibrahim, M.R. Hassan, Towards an aerogel based coating for aerospace applications: reconstituting aerogel particles via spray drying, IOP Conf. Ser. Mater. Sci. Eng. 152 (2016). https://doi.org/10.1088/1757-899X/152/1/012066.
[11] N. Bheekhun, A.R. Abu Talib, M.R. Hassan, Tailoring aerogel for thermal spray applications in aero-engines: A screening study, Adv. Mater. Sci. Eng. 2018 (2018). https://doi.org/10.1155/2018/5670291.
[12] S.M. Jones, Non-silica aerogels as hypervelocity particle capture materials, Meteorit. Planet. Sci. 45 (2010) 91–98. https://doi.org/10.1111/j.1945-5100.2009.01007.x.
[13] S. Yoon, G.D. Han, D.Y. Jang, J.W. Kim, D.H. Kim, J.H. Shim, Fabrication of yttria-stabilized zirconia aerogel for high-performance thermal barrier coating, J. Alloys Compd. 806 (2019) 1430–1434. https://doi.org/10.1016/j.jallcom.2019.07.156.
[14] F.I. Hurwitz, M. Gallagher, T.C. Olin, M.K. Shave, M.A. Ittes, K.N. Olafson, M.G. Fields, H. Guo, R.B. Rogers, Optimization of alumina and aluminosilicate aerogel structure for high-temperature performance, Int. J. Appl. Glas. Sci. 5 (2014) 276–286. https://doi.org/10.1111/ijag.12070.
[15] C. Folgar, D. Folz, C. Suchicital, D. Clark, Microstructural evolution in silica aerogel, (2007). https://doi.org/10.1016/j.jnoncrysol.2007.02.047.

[16] S. Rezaee, K. Ranjbar, A.R. Kiasat, The effect of surfactant on the sol–gel synthesis of alumina-zirconia nanopowders, Ceram. Int. 44 (2018) 19963–19969. https://doi.org/10.1016/j.ceramint.2018.07.263.
[17] H.N.R. Jung, W. Han, H.H. Cho, H.H. Park, Effect of cationic and non-ionic surfactants on the microstructure of ambient pressure dried zirconia aerogel, Mater. Express. 7 (2017) 291–298. https://doi.org/10.1166/mex.2017.1371.
[18] E. Ruckenstein, R. Nagarajan, Critical micelle concentration. A transition point for micellar size distribution, J. Phys. Chem. 79 (1975) 2622–2626. https://doi.org/10.1021/j100591a010.
[19] C.N. Chervin, B.J. Clapsaddle, H.W. Chiu, A.E. Gash, J.H. Satcher, S.M. Kauzlarich, Aerogel synthesis of yttria-stabilized zirconia by a non-alkoxide sol-gel route, Chem. Mater. 17 (2005) 3345–3351. https://doi.org/10.1021/cm0503679.
[20] C.M.R. Almeida, M.E. Ghica, L. Durães, An overview on alumina-silica-based aerogels, Adv. Colloid Interface Sci. 282 (2020). https://doi.org/10.1016/j.cis.2020.102189.
[21] R.C. Walker, A.E. Potochniak, A.P. Hyer, J.K. Ferri, Zirconia aerogels for thermal management: Review of synthesis, processing, and properties information architecture, Adv. Colloid Interface Sci. 295 (2021) 102464. https://doi.org/10.1016/J.CIS.2021.102464.
[22] B. Liu, X. Liu, X. Zhao, H. Fan, J. Zhang, X. Yi, M. Gao, L. Zhu, X. Wang, High-strength, thermal-stable ZrO2 aerogel from polyacetylacetonatozirconium, Chem. Phys. Lett. 715 (2019) 109–114. https://doi.org/10.1016/j.cplett.2018.11.025.
[23] J. Chevalier, L. Gremillard, A. V. Virkar, D.R. Clarke, The tetragonal-monoclinic transformation in zirconia: Lessons learned and future trends, J. Am. Ceram. Soc. 92 (2009) 1901–1920. https://doi.org/10.1111/J.1551-2916.2009.03278.X.
[24] H. Sai, L. Xing, J. Xiang, F. Zhang, L. Cui, X. Liang, B. Song, C. Zhao, Z. Li, Effects of surfactants on the synthesis of silica aerogels prepared by ambient pressure drying, in: Key Eng. Mater., Trans Tech Publications Ltd, 2012: pp. 1625–1630. https://doi.org/10.4028/www.scientific.net/KEM.512-515.1625.
[25] S. Huang, X. Wu, Z. Li, L. Shi, Y. Zhang, Q. Liu, Rapid synthesis and characterization of monolithic ambient pressure dried MTMS aerogels in pure water, J. Porous Mater. 27 (2020) 1241–1251. https://doi.org/10.1007/s10934-020-00902-3.
[26] F.I. Hurwitz, R.B. Rogers, H. Guo, A. Garg, N.S. Olson, D. Phan, J.L. Cashman, Phase development and pore stability of yttria- and ytterbia-stabilized zirconia aerogels, J. Am. Ceram. Soc. (2020). https://doi.org/10.1111/jace.17376.
[27] N.S. Olson, F.I. Hurwitz, H. Guo, N.J. Madden, J.L. Stokes, R.B. Rogers, J.A. Krogstad, Enhanced thermal stability of high yttria concentration YSZ aerogels, J. Am. Ceram. Soc. 104 (2021) 4190–4202. https://doi.org/10.1111/jace.17792.
[28] W. Li, Y.C. Han, J.L. Zhang, L.X. Wang, J. Song, Thermodynamic modeling of CTAB aggregation in water-ethanol mixed solvents, Colloid J. 68 (2006) 304–310. https://doi.org/10.1134/S1061933X06030069.
[29] M. Rabiei, A. Palevicius, A. Monshi, S. Nasiri, A. Vilkauskas, G. Janusas, Comparing methods for calculating nano crystal size of natural hydroxyapatite using

X-ray diffraction, Nanomaterials. 10 (2020) 1–21. https://doi.org/10.3390/nano10091627.
[30] N.C. Das, H. Cao, H. Kaiser, G.T. Warren, J.R. Gladden, P.E. Sokol, Shape and size of highly concentrated micelles in CTAB/NaSal solutions by small angle neutron scattering (SANS), Langmuir. 28 (2012) 11962–11968. https://doi.org/10.1021/la2022598.
[31] V. Patel, N. Dharaiya, D. Ray, V.K. Aswal, P. Bahadur, PH controlled size/shape in CTAB micelles with solubilized polar additives: A viscometry, scattering and spectral evaluation, Colloids Surfaces A Physicochem. Eng. Asp. 455 (2014) 67–75. https://doi.org/10.1016/j.colsurfa.2014.04.025.
[32] G. Witz, V. Shklover, W. Steurer, S. Bachegowda, H.P. Bossmann, Phase evolution in yttria-stabilized zirconia thermal barrier coatings studied by rietveld refinement of X-ray powder diffraction patterns, J. Am. Ceram. Soc. 90 (2007) 2935–2940. https://doi.org/10.1111/J.1551-2916.2007.01785.X.
[33] D.N. Rubingh, P.M. Holland, Cationic Surfactants: Physical Chemistry, 1st ed., M. Dekker, New York, New York, 1991.
[34] M. Kurahashi, K. Kanamori, K. Takeda, H. Kaji, K. Nakanishi, Role of block copolymer surfactant on the pore formation in methylsilsesquioxane aerogel systems, RSC Adv. 2 (2012) 7166–7173. https://doi.org/10.1039/C2RA20799K.
[35] N. Baccile, G. Laurent, C. Bonhomme, P. Innocenzi, F. Babonneau, Solid-state NMR characterization of the surfactant−silica interface in templated silicas: Acidic versus basic conditions, Chem. Mater. 19 (2007) 1343–1354. https://doi.org/10.1021/CM062545J.
[36] Y. Yu, F.P. Du, J.C. Yu, Y.Y. Zhuang, P.K. Wong, One-dimensional shape-controlled preparation of porous Cu2O nano-whiskers by using CTAB as a template, J. Solid State Chem. 177 (2004) 4640–4647. https://doi.org/10.1016/J.JSSC.2004.10.025.

Tables

Table 1. BET surface area and BJH desorption cumulative pore volume of YSZ aerogels at varying CTAB levels and heat-treatment conditions. BET surface area (m^2/g) and BJH desorption cumulative pore volume (cm^3/g) of YSZ aerogels at varying CTAB levels (0x CTAB, 0.5x CTAB, and 2x CTAB) and heat-treatment conditions (as-dried, 600°C, 1000° C) measured using nitrogen adsorption/desorption.

	BET Surface Area (m^2/g)			**BJH Desorption Cumulative Pore Volume (cm^3/g)**		
	0x CTAB	0.5x CTAB	2x CTAB	0x CTAB	0.5x CTAB	2x CTAB
As-Dried	263	403	407	0.97	1.95	1.43
600°C	149	257	181	0.77	1.35	0.88
1000°C	37	52	47	0.20	0.36	0.21

Table 2. Average crystallite size of YSZ aerogels at various CTAB levels and heat-treatment conditions. Average crystallite size values (Å) for 0x CTAB, 0.5x CTAB, and 2x CTAB YSZ aerogels at 600°C and 1000 °C determined through XRD and TEM analysis. Four different equations were used to determine the crystallite size following XRD analysis.

		Average Crystallite Size (Å)				
CTAB	**Temperature (°C)**	Scherrer	Monshi-Scherrer (M-S)	Williamson-Hall (W-H)	Size-Strain-Plot (SSP)	TEM Analysis
0x	600	55	60	68	63	61
	1000	197	227	283	250	270
0.5x	600	56	60	65	62	73
	1000	195	210	225	205	217
2x	600	55	59	64	60	76
	1000	193	200	207	201	210

Figures/Schemes with captions (All to be printed in color)

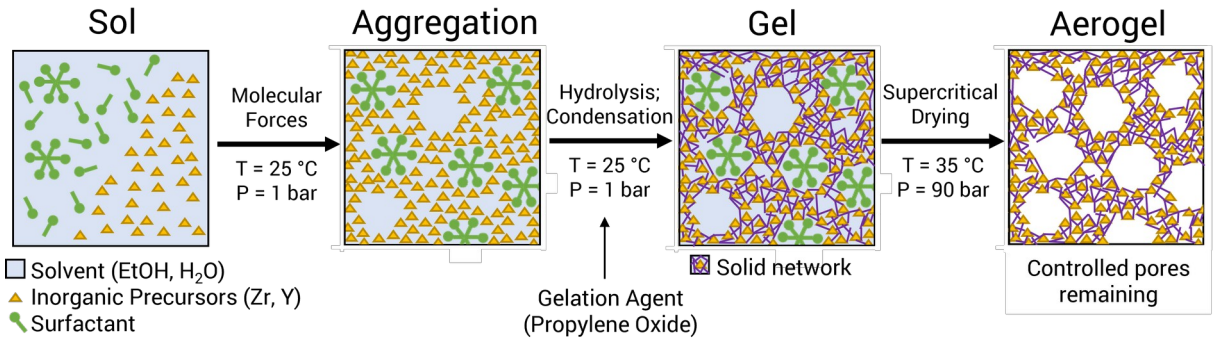

Scheme 1. Surfactant templating during sol-gel synthesis of aerogels. Following formulation of the sol, precursors aggregate surrounding surfactant micelles, forming a solid gel network; surfactants are removed from the aerogel network through washing, supercritical drying and/or heat-treatment, leaving behind tunable, uniform pores.

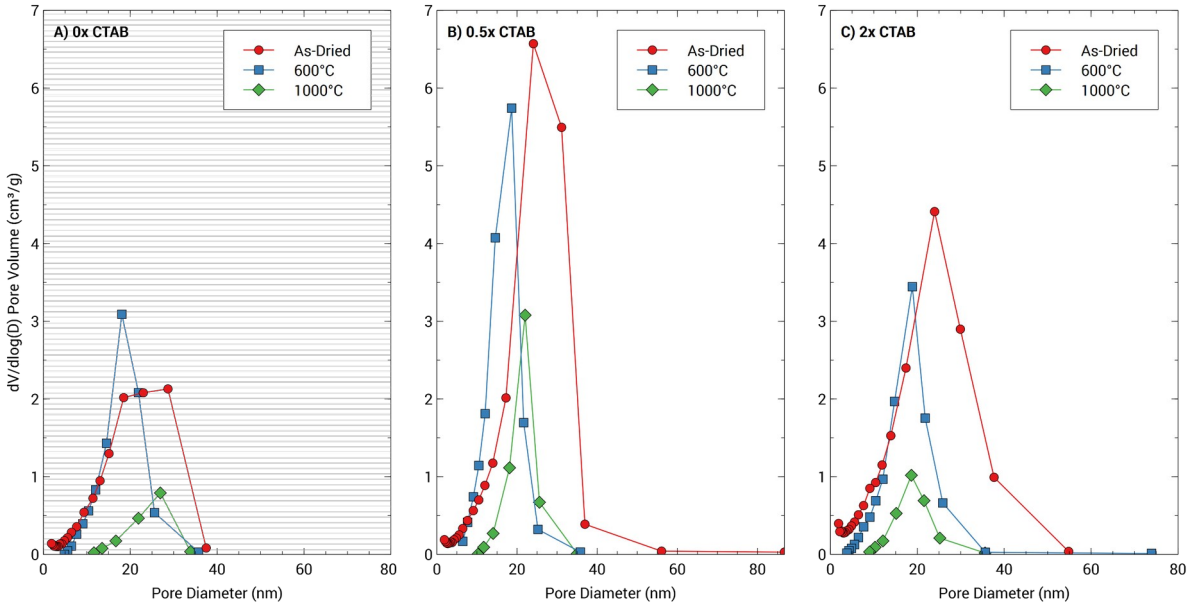

Figure 1. Pore size distributions of YSZ aerogels with varying CTAB levels and heat-treatment. Pore size distributions of YSZ aerogels at A) 0x CTAB, B) 0.5x CTAB, and C) 2x CTAB at different heat-treatment conditions (as-dried (circle), 600°C (square), and 1000° C (diamond)).

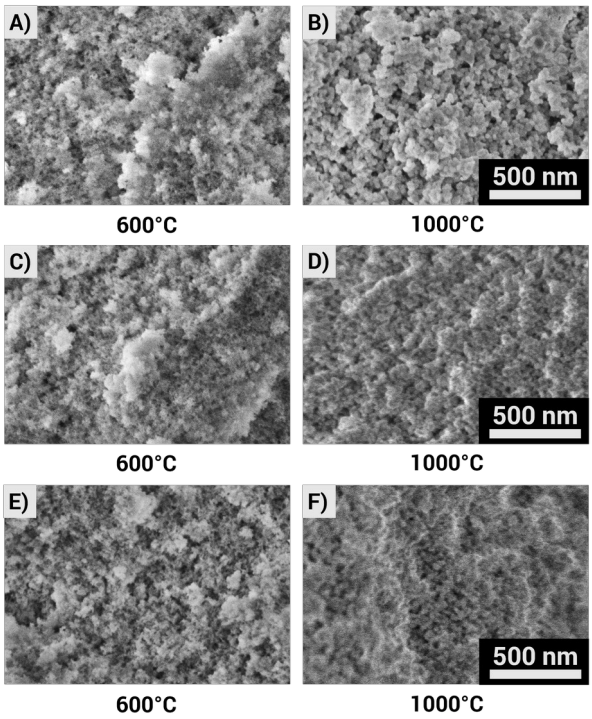

Figure 2. SEM images of YSZ aerogels with varying CTAB levels and heat-treatment. SEM images of YSZ aerogels at two different heat-treatment conditions, 600°C (left) and 1000°C (right), for aerogels with A,B) 0x CTAB, C, D) 0.5x CTAB, and E, F) 2x CTAB.

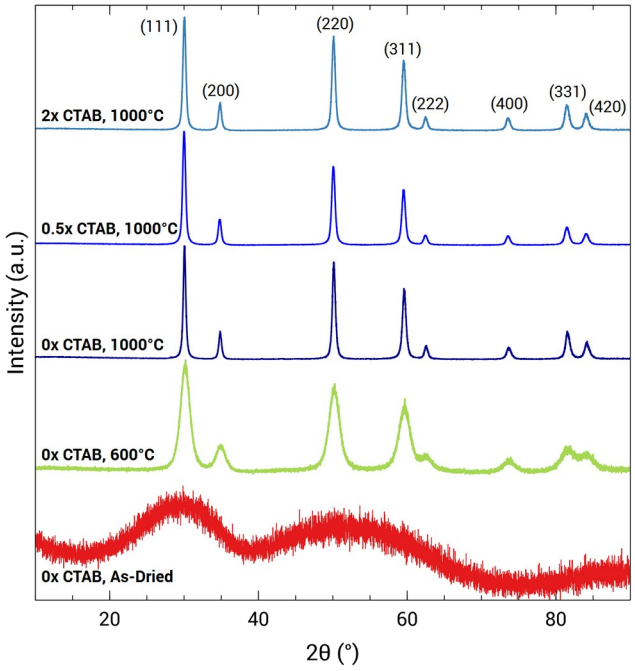

Figure 3. XRD patterns at various levels of CTAB and heat-treatment conditions. XRD patterns for YSZ aerogels with 0x CTAB, 0.5x CTAB, and 2x CTAB at various heat-treatment conditions of as-dried, 600°C, and 1000°C. The Miller indices (hkl values) are displayed at the top of the figure.

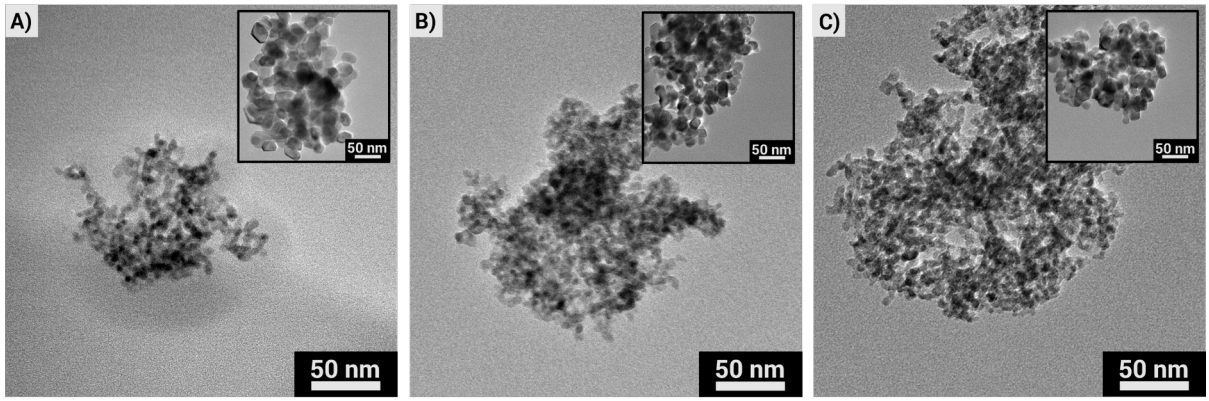

Figure 4. TEM images of YSZ aerogels at various levels of CTAB and heat-treatment conditions. TEM images at 100k magnification of YSZ aerogels with A) 0x CTAB, B) 0.5x CTAB, and C) 2x CTAB that have been heat-treated at 600°C and 1000°C (inset).

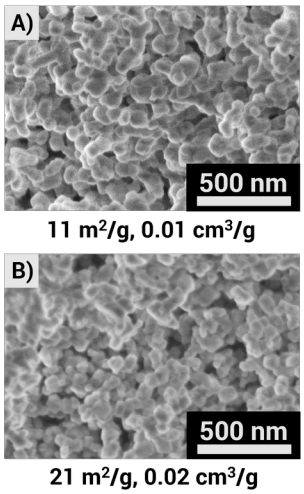

Figure 5. SEM images of YSZ aerogels at 1100°C with varying CTAB levels. SEM images of YSZ aerogels with A) 0x CTAB and B) 2x CTAB that were heat-treated at 1100°C. BET surface area and BJH desorption cumulative pore volume values are also displayed.